Pressure Response of Aanderaa and Sea-Bird Oxygen Optodes

Henry C. Bittig and Björn Fiedler

Marine Biogeochemistry Department, GEOMAR Helmholtz Centre for Ocean Research Kiel, Kiel, Germany

Peer Fietzek

Marine Biogeochemistry Department, GEOMAR Helmholtz Centre for Ocean Research Kiel, and Kongsberg Maritime Contros GmbH, Kiel, Germany

Arne Körtzinger

Marine Biogeochemistry Department, GEOMAR Helmholtz Centre for Ocean Research Kiel, Kiel, Germany

ABSTRACT

This study investigated the effect of hydrostatic pressure of up to 6000 dbar on Aanderaa and Sea-Bird oxygen optodes both in the laboratory and in the field. The overall pressure response is a reduction in the O_2 reading by 3%–4% per 1000 dbar, which is closely linear with pressure and increases with temperature. Closer inspection reveals two superimposed processes with an opposite effect: an O_2-independent pressure response on the luminophore that increases optode O_2 readings and an O_2-dependent change in luminescence quenching that decreases optode O_2 readings. The latter process dominates and is mainly due to a shift in the equilibrium between the sensing membrane and seawater under elevated pressures. If only the dominant O_2-dependent process is considered, then the Aanderaa and Sea-Bird optodes differ in their pressure response. Compensation of the O_2-independent process, however, yields a uniform O_2 dependence for Aanderaa optodes with standard foil and fast-response foil as well as for Sea-Bird optodes. A new scheme to calculate optode O_2 from raw data is proposed to account for the two processes. The overall uncertainty of the optode pressure correction amounts to 0.3% per 1000 dbar, which is mainly due to variability between the sensors.

1. Introduction

Oxygen optodes have become a core element of autonomous biogeochemical observations (Johnson et al. 2009). There is rarely a biogeochemical field study that does not measure oxygen (e.g., Fennel et al. 2011; Johnson et al. 2010) because of its core character within fundamental biogeochemical processes, that is, primary production, respiration, and oxidation. The focus of this work is placed on the processing of oxygen optode data with regard to the effects of hydrostatic pressure.

Sensor measurements essentially encompass two separate steps:

Step 1: Data acquisition, that is, the transfer of an environmental state to sensor raw data, for example, the optode's lifetime information.

Step 2: Translation of the raw sensor data to the parameter of interest, that is, O_2 content in our case.

The second step relies on a functional model that mimics the physics of the sensing principle (and the sensor design). For oxygen optodes, the temperature dependence and the pressure dependence are usually dealt with separately and several functional models are in use (see below). Despite some differences, all of them succeed in relating the sensor output—that is, the optode raw data plus salinity and pressure measurements—with the target variable, a temperature-, salinity-, and pressure-corrected O_2 value, either expressed as oxygen concentration c_{O_2} or partial pressure pO_2.

The temperature-dependent part of the functional model has received quite some attention in recent years. It evolved from a polynomial approach (e.g., Aanderaa Data Instruments 2009, appendix 6) over variants of a Stern–Volmer inspired, parametric function (Uchida et al. 2008, 2010; Sea-Bird Electronics 2013) to a model approximating two-site physics (McNeil and D'Asaro 2014). The calculated oxygen quantity is either the (freshwater) c_{O_2} (Aanderaa Data Instruments 2009; Uchida et al. 2008; Sea-Bird Electronics 2013), which requires subsequent salinity correction, or the pO_2 (Bittig et al. 2012; McNeil and D'Asaro 2014), which can be converted to concentration via the oxygen solubility $c^*_{O_2}$ (Garcia and Gordon 1992) [see Eq. (6) in section 2a].

The pressure correction, in contrast, is only poorly constrained. Laboratory experiments of Aanderaa optodes provided a linear dependence of optode c_{O_2} on hydrostatic pressure P,

$$c_{O_2} = c_{O_2,\text{raw}}(1 + f\,P), \tag{1}$$

where f is 4% per 1000 dbar (Tengberg et al. 2006). A field study by Uchida et al. (2008) refined this number to 3.2% per 1000 dbar, which is generally used for these sensors today (e.g., Thierry et al. 2013). Sea-Bird Electronics SBE63 optodes use a temperature- and pressure-dependent exponential equation,

$$c_{O_2} = c_{O_2,\text{raw}} \exp\left(\frac{0.011\,\text{K dbar}^{-1}\,P}{\vartheta + 273.15\,\text{K}}\right), \tag{2}$$

with temperature ϑ (°C) (Sea-Bird Electronics 2013), which comes down to approximately 4% per 1000 dbar.

The Tengberg et al. (2006) results are based on few pressure cycles and three Aanderaa optodes with closely succeeding serial numbers—that is, a similar history—only. The Uchida et al. (2008) study is somewhat more extensive in that it used 11 Aanderaa optodes at a total of 279 hydrocasts with Winkler-based oxygen titrations on 8047 discrete samples. This dataset, however, is dominated by one individual sensor (255 casts, 7234 Winkler samples). There is no study known to us that deals with the pressure response of SBE63 optodes.

The aim of this study is as follows:

- to reinvestigate the pressure dependence of Aanderaa and Sea-Bird optodes using both laboratory and field experiments,
- to properly separate pressure from temperature effects on the optode pressure response,
- to reevaluate and improve existing pressure-correction algorithms, and
- to characterize the error associated with the pressure correction.

This manuscript first deals with some theoretical background on the conversion of oxygen quantities and the relation between pressure and luminescence quenching. Then the laboratory and field experiments are presented and a pressure-correction rationale is derived from the results. Finally, the pressure response of the Aanderaa and Sea-Bird optodes and its uncertainty is quantified.

2. Background

a. Oxygen quantity conversion

Oxygen saturation can be expressed in terms of oxygen concentration, as the ratio of c_{O_2} to O_2 solubility $c^*_{O_2}$, and in terms of partial pressure, as the ratio of water pO_2 to the atmospheric equilibrium partial pressure $pO_{2,\text{air}}$,

$$O_2\text{sat.} = \frac{c_{O_2}}{c^*_{O_2}} = \frac{pO_2}{pO_{2,\text{air}}}. \tag{3}$$

Equation (3) can thus be used to easily convert between concentrations and partial pressures.

At the sea surface, $pO_{2,\text{air}}$ follows

$$pO_{2,\text{air}} = \chi O_2(p_{\text{air}} - pH_2O), \tag{4}$$

where pH_2O is the saturation water vapor pressure after Weiss and Price (1980) and $\chi O_2 = 0.209\,46$ is the mixing ratio of O_2 in dry air (Glueckauf 1951). Term $pO_{2,\text{air}}$ and thus O_2 saturation are therefore dependent on the ambient atmospheric pressure p_{air}. The temperature (ϑ)- and salinity (S)-dependent seawater O_2 solubility $c^*_{O_2}(\vartheta, S)$ is given for a pressure of 1 atm (Garcia and Gordon 1992) and needs to be scaled to ambient pressure for surface applications according to

$$c^*_{O_2}(\vartheta, S, p_{\text{air}}) = c^*_{O_2}(\vartheta, S) \frac{p_{\text{air}} - pH_2O(\vartheta, S)}{1013.25\,\text{mbar} - pH_2O(\vartheta, S)} \tag{5}$$

to give a proper saturation [Eq. (3)]. In the above equation, only components other than water vapor are scaled since pH_2O depends on temperature and salinity only but not on p_{air}.

Inserting Eqs. (4) and (5) into Eq. (3) yields

$$c_{O_2} = \frac{c^*_{O_2}(\vartheta, S)}{\chi O_2[1013.25\,\text{mbar} - pH_2O(\vartheta, S)]} pO_2, \tag{6}$$

that is, the conversion of pO_2 to O_2 concentration c_{O_2} is independent of p_{air} (since the change in O_2 saturation cancels out).

Below the surface, hydrostatic pressure P affects both the oxygen solubility and partial pressure. Enns et al. (1965) describe an exponential increase in pO_2 of about 14% per 1000 dbar and Taylor (1978) gives a theoretical relationship,

$$pO_2(P) = pO_2 \exp\left[\frac{V_m(O_2)\, P}{R(\vartheta + 273.15\,\text{K})}\right], \qquad (7)$$

where $V_m(O_2) = 31.7\,\text{mL mol}^{-1}$ is the molar volume of O_2 in seawater (Enns et al. 1965) and $R = 8.314\,\text{J mol}^{-1}\,\text{K}^{-1}$ is the universal gas constant. The pO_2 increase with hydrostatic pressure reflects a higher outgassing tendency with depth, that is, a reduced solubility $c_{O_2}^*(\vartheta, S, P)$. Consequently, Eqs. (7) and (6) need to be combined for the conversion between $pO_2(P)$ and c_{O_2} for subsurface applications.

b. Pressure, chemical potential, and luminescence quenching

The rationale behind the pressure dependence of pO_2 and $c_{O_2}^*$ is nicely discussed in Ludwig and Macdonald (2005) and in parts reproduced below.

The chemical potential μ_i of a species i determines its ability to act in a chemical reaction or state transition. It is defined as

$$\mu_i = \mu_i^* + RT \ln a_i, \qquad (8)$$

where a_i is the activity of the species and μ_i^* is the chemical potential of an (imaginary) standard state at the same temperature T (kelvins) and P. For dissolved oxygen, the standard state is chosen according to Henry's law to be an ideal solution where O_2 is infinitely diluted in the solvent. In that state, activity a_i equals concentration c_i and the activity coefficient γ_i is 1,

$$a_i = \gamma_i c_i, \quad \gamma_i \to 1 \quad \text{for} \quad c_i \to 0. \qquad (9)$$

According to this definition, activity is an effective concentration and includes only solute–solute interactions but no solute–solvent or solvent–solvent interactions (see case i in Ludwig and Macdonald 2005).

From thermodynamics, the pressure dependence of the chemical potential μ_i is

$$\left(\frac{\partial \mu_i}{\partial P}\right)_T = V_{m,i}, \qquad (10)$$

where $V_{m,i}$ is the partial molar volume of the species i, that is, pressure increases the chemical potential μ_i. The combination of Eqs. (8) and (10) gives

$$\left(\frac{\partial \mu_i}{\partial P}\right)_T = V_{m,i} = \left(\frac{\partial \mu_i^*}{\partial P}\right)_T + RT\left(\frac{\partial \ln a_i}{\partial P}\right)_T$$

$$V_{m,i} = V_{m,i}^* + RT\left(\frac{\partial \ln a_i}{\partial P}\right)_T, \qquad (11)$$

where $V_{m,i}^*$ is the partial molar volume at infinite dilution (i.e., in the imaginary standard state) and $V_{m,i}$ is the actual partial molar volume. Experimental data show no apparent difference of V_{m,O_2} in seawater or freshwater (Enns et al. 1965) and there is no concentration dependence (cf. Ludwig and Macdonald 2005), that is, $V_{m,i}$ is not significantly different from $V_{m,i}^*$.

Thus, the concentration (and activity) stays nearly unchanged upon pressurization and the main pressure effect is on the chemical potential of the reference state μ_i^* (see case i in Ludwig and Macdonald 2005). As a consequence, the solubility changes with pressure. The change in μ_i^* and solubility accounts for the structural effect of pressure (on solute–solvent and solvent–solvent interactions). This is reflected in the higher outgassing tendency of O_2 with pressure [increased pO_2; Eq. (7); Enns et al. 1965].

There is some confusion in the literature about the pressure effect on luminescence quenching by oxygen. Since pO_2 increases significantly (ca. 14% per 1000 dbar), one would assume luminescence quenching to increase concurrently (e.g., Taylor 1978; McNeil and D'Asaro 2014). However, no such effect is observed for a luminophore in solution (Carey and Gibson 1976). Instead, the authors see a small increase in fluorescence intensity (5% at 10 000 dbar) attributed to the compression of the solution.

The reason for this at first counterintuitive observation is that dynamic quenching by O_2 is a diffusion-controlled process (see Lakowicz 2006). The diffusion of oxygen is driven by the gradient in chemical potential and retarded by frictional resistance. Pressure increases μ_i [Eq. (10)], however, it is shifted by the same amount throughout the solvent (since $V_{m,i}$ is the same) and the gradient of μ_i remains constant, that is, quenching in solution stays the same. The observed marginal increase in fluorescence (Carey and Gibson 1976) can be attributed to changes in geometry (and thus the concentration) as well as viscosity upon compression.

In the case of oxygen optodes, the situation is slightly more complicated since phase equilibrium is involved: The luminophore is embedded in a silicone sensing membrane (^{M}) that is in equilibrium with the ambient liquid seawater (^{L}) with equilibrium condition

$$\mu^M = \mu^L. \qquad (12)$$

With Eq. (8), this yields

$$\mu^{*,M} + RT \ln a^M = \mu^{*,L} + RT \ln a^L, \quad (13)$$

where $\mu^{*,M}$ and $\mu^{*,L}$ refer to the standard state in the membrane and liquid, respectively (i.e., they are different). The pressure dependence at equilibrium follows

$$V_m^{*,M} + RT\left(\frac{\partial \ln a^M}{\partial P}\right)_T = V_m^{*,L} + RT\left(\frac{\partial \ln a^L}{\partial P}\right)_T. \quad (14)$$

The ambient seawater as bulk liquid will determine the location of the equilibrium (as a result of its relative size). Following the same argument as given above, its activity a^L will remain constant, that is, $\partial \ln a^L/\partial P = 0$. Equation (14) simplifies to

$$\left(\frac{\partial \ln a^M}{\partial P}\right)_T = \frac{V_m^{*,L} - V_m^{*,M}}{RT}, \quad (15)$$

which upon integration from $P = 0$ dbar gives

$$a^M(P) = a^M \exp\left[\frac{(V_m^{*,L} - V_m^{*,M})P}{RT}\right]. \quad (16)$$

Pressure changes the partitioning of the equilibrium and thus the membrane O_2 concentration (activity) because of a difference in the partial molar volumes. In seawater $V_m^L(O_2) = 31.7 \text{ mL mol}^{-1}$ (Enns et al. 1965), while $V_m^M(O_2)$ in the silicone sensing membrane is larger (39 mL mol^{-1}, Kamiya et al. 1990; 46 mL mol^{-1}, Kamiya et al. 2000). Accordingly, the O_2 concentration inside the sensing membrane (which is relevant for luminescence quenching) is reduced by ca. 3.0% or 5.5% per 1000 dbar. The optodes are thus expected to show a lower O_2 under pressure. This equilibrium effect is slightly stronger at low temperatures [see Eq. (16)].

If geometry/viscosity changes are included, then compression leads to both a subtle increase in O_2 concentration (order of 0.4% per 1000 dbar; Jordan and Koros 1990) and an increase in viscosity of the sensing membrane. The latter causes oxygen diffusivity to decrease and luminescence quenching as a diffusion-controlled process thus becomes less efficient (Lakowicz 2006). Therefore, lifetimes (phase shift, phase delay) are higher and there appears to be less O_2 detected by the optode. However, we consider the μ-increase-caused re-equilibration of O_2 between the sensing membrane and ambient water to be the main driver for the optode pressure response, rather than changes in concentration or diffusivity. In fact, silicone is mostly compressed at hydrostatic pressures of 10 dbar, so any effect on physical compression or diffusivity should be limited to mostly the 0–10-dbar range. Still, these effects are superimposed onto the equilibrium effect and may alter the temperature dependence of the pressure response.

3. Methods

a. Laboratory experiments

Two laboratory experiments were performed in March and August 2012 at the high pressure vessel facility of the Technology and Logistics Centre of GEOMAR. The first experiment employed six Aanderaa 3830 optodes and one Aanderaa 4330F optode up to a pressure of 6000 dbar at ca. 4° and 18°C. The second experiment used five Aanderaa 4330 optodes, two Sea-Bird SBE63 optodes, and one of the Aanderaa 3830 optodes of the first experiment up to a pressure of 2000 dbar at ca. 8°, 15°, and 24°C. The sensors varied considerably in age (0.5–9 yr) and their deployment history (newly manufactured vs repeated CTD or multiyear mooring deployments).

The pressure vessel interior (ca. 30-cm diameter, 93-cm height) was split into two separate freshwater-filled volumes by using a commercial watertight dry bag. Thus, contamination of the inside volume by oil spills from the hydraulic pump was prevented. After closure of the dry bag, the water was cooled to cause undersaturation and left to stand for at least 2.5 days (unpressurized) or 12 h (pressurized) to ensure complete dissolution of accidentally trapped air bubbles. The tank was pressurized by means of a hydraulic pump (type EH 1H, LEWA GmbH) with a compression rate around 10 dbar s^{-1}. Decompression at a similar rate was achieved by slowly opening a vent valve. The whole pressure vessel was temperated/cooled with an external heat exchanger and a cryostat (Julabo GmbH). The lower temperature limit was determined by the room temperature of the workshop as a result of diffusive warming of the tank.

The sensors were attached to a holding frame and put into the dry bag inside the pressure vessel, that is, the inner volume. An SBE 5T pump was added to homogenize the inner volume. During the experiment, optodes were in part powered and logged online through a cable connection and in part supplied offline by custom-made loggers. The dry bag was sealed tightly around the cables by means of a stainless steel hose clamp. The logging interval was set to 30 s (online) or 60 s (offline).

Pressure cycles were designed as follows: After 20 min at zero pressure, the tank was pressurized and held at the desired pressure level for 20 min before being depressurized again. Subsequently, it was kept at zero pressure
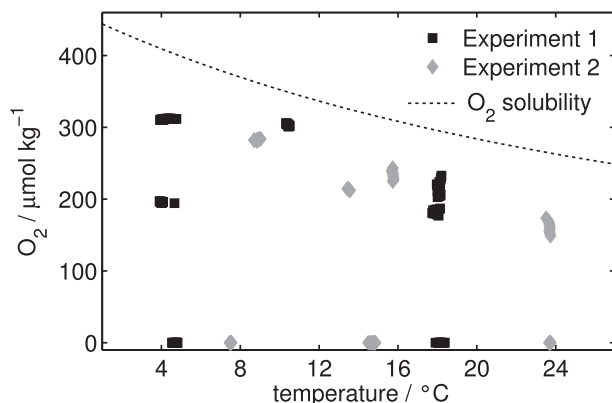
FIG. 1. Temperature and oxygen concentration during laboratory experiment 1 (squares) and experiment 2 (diamonds). The dotted line denotes the O_2 solubility (Garcia and Gordon 1992).

for 20 min again. The first experiment used pressure levels at 500, 1000, 2000, 4000, and 6000 dbar, while the second experiment had pressure levels at 700, 1400, and 2000 dbar. During each pressure cycle, water temperatures increased/decreased because of near-adiabatic compression/decompression by ca. 0.15°C per 1000 dbar.

Different oxygen levels were used: Pressure cycles at ca. 80% O_2 saturation served as the high end member in both experiments. For a zero end member, O_2 was consumed in the inner volume by the addition of a stoichiometric amount of Na_2SO_3 to the dry bag. In addition, the first experiment featured an intermediate level at ca. 55% O_2 saturation and 4°C, a third temperature (10°C) at 80% O_2 saturation, and a repetition at 18°C and 80% O_2 (see Fig. 1 for an overview). Each pressure cycle was repeated three to four times at each temperature and oxygen level.

For the first experiment, three out of the seven Aanderaa optodes were individually laboratory calibrated according to Bittig et al. (2012), while all five Aanderaa optodes and one of the two SBE63 optodes were laboratory calibrated in the second experiment (see Table 1). Their average O_2 reading, validated against Winkler samples at the beginning and end of each experiment, served as reference for the other factory-batch-calibrated optodes.

b. Field experiment

During R/V Polarstern cruise ANT-XXVII/2 (Rohardt et al. 2011) to the Southern Ocean, two Aanderaa optodes were attached to the CTD, a standard model 3830 optode, and a fast-response model 4330F optode. Both were individually multipoint calibrated before the cruise in October 2010 and recalibrated afterward in July 2011 and showed no sign of drift (see Bittig et al. 2012). Laboratory

TABLE 1. Overview of the optodes used during the laboratory experiments 1 and 2: Optode type and serial number, manufacture date (date of factory calibration) as a proxy of the age of the sensor, date of the laboratory calibration, and which sensor was used in which laboratory experiment. Optodes 3830 529 and 4330F 207 were also used in the field experiment on board R/V Polarstern cruise ANT-XXVII/2 (December 2010–January 2011).

Optode	Manufacture date	Date of lab calibration	Expt 1 Mar 2012	Expt 2 Aug 2012
3830 203	Feb 2003[a]	Jul 2011	x	x
3830 529	Dec 2004[a]	Apr 2012	x	
3830 938	Sep 2007		x	
3830 942	Sep 2007		x	
3830 1067	Jul 2008[b]		x	
3830 1143	Dec 2008		x	
4330F 207[c]	Sep 2009	Dec 2011	x	
4330 845	Dec 2011	Jul 2012		x
4330 849	Dec 2011	Jul 2012		x
4330 850	Dec 2011	Dec 2012		x
4330 853[c]	Dec 2011	Jan 2013		x
4330 856	Dec 2011	Dec 2012		x
SBE63 23[c]	Mar 2012			x
SBE63 115[c]	Mar 2012	Apr 2013		x

[a] Sensor foil replaced in July 2008 (foil batch date June 2007).
[b] Sensor foil replaced in November 2010 (foil batch date February 2010).
[c] Online sensor at 30-s intervals; all other sensors at 60-s intervals.

calibrations were linearly adjusted to a total of 2296 Winkler samples at 122 stations.

The ANT-XXVII/2 Southern Ocean field setting covers a very narrow temperature range (Fig. 2). With cold water temperatures throughout the entire water column, the pressure response can be evaluated independently from a possible temperature effect.

Response times τ for the 3830 and 4330F optode are on the order of 25 and 8 s, respectively, and both sensors sampled at 5-s intervals. The response time effect was removed following the procedures of Bittig et al. (2014) by using a temperature-dependent τ parameterization of the mode response time derived for this cruise (see Fig. 6a in Bittig et al. 2014). For the fast-response 4330F optode, there is no significant difference between uncorrected and τ-corrected data. The response time correction of the 3830 optode, however, improves data quality significantly by removing artifacts caused by the sensor's slow response, for example, the low bias around the surface oxycline (Fig. 2).

4. Results

a. Laboratory experiments

During the experiments, oxygen levels showed a small and steady drift on the order of -1 to $-3\,\mu\text{mol}\,\text{kg}^{-1}\,\text{h}^{-1}$
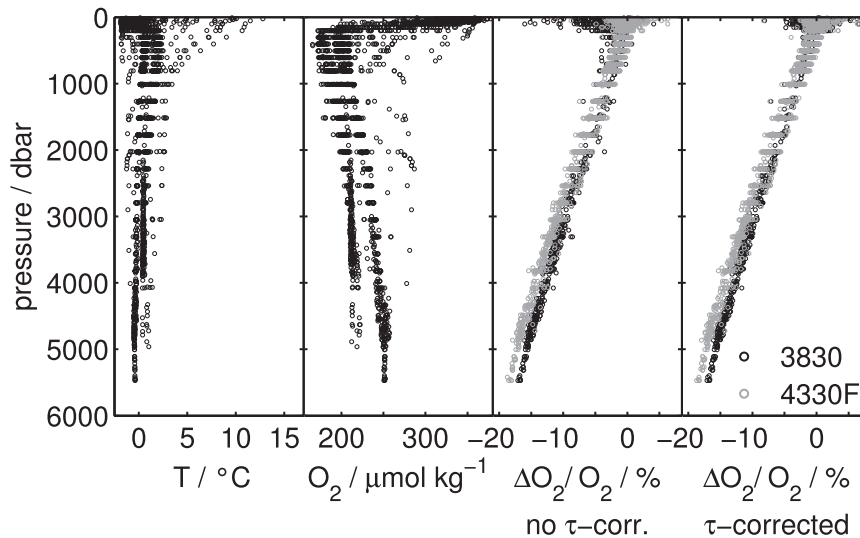
FIG. 2. Field conditions and difference between optode O_2 and Winkler O_2 during R/V *Polarstern* cruise ANT-XXVII/2. (from left to right) Temperature, Winkler O_2, O_2 difference using uncorrected optode data, and O_2 difference using τ-corrected optode data (model 3830 in black, model 4330F in gray). Response time τ correction removes the systematic low bias for the 3830 optode around the surface oxycline, while data of the 4330F optode remain unaffected. Term ΔO_2 follows a linear trend relative to optode O_2 (third and fourth panels).

for unknown reasons. It may be related to the combination of different metals (surface of the pressure vessel, sensor housings, screws) or to bacterial respiration inside the enclosed volume. The drift was accounted for by detrending the data before analysis of the pressure response.

Despite the very high (de-)compression rates, the optode pressure response was near instantaneous (within the 60-s resolution) and fully reversible. Reequilibration between the sensing membrane and ambient liquid [Eq. (16)] thus appears to happen on faster time scales than pressure changes. Since the repartitioning/equilibration effect is an optode phenomenon, it is merged into the optode pressure response in the following discussion and is not accounted for separately.

Optodes show a different behavior at high O_2 and at very low O_2 (Figs. 3a,b, respectively). At high O_2, lifetime (phase shift, phase delay) increases with hydrostatic pressure and O_2 readings are lower (ca. 3%–4% per 1000 dbar). At zero O_2, lifetime decreases with hydrostatic pressure and O_2 and readings are thus apparently higher (ca. $0.3\,\mu\mathrm{mol\,kg^{-1}}$ per 1000 dbar, being more pronounced at low temperatures). The two opposing effects cancel at around 10 mbar (5% O_2 saturation), that is, the apparent reduction of O_2 is dominant in most applications.

b. Pressure correction rationale

Having a reduced O_2 slope/sensitivity under elevated pressure and a simultaneous opposite effect in the

absence of O_2 is very similar to observations of optode drift behavior (Bittig and Körtzinger 2015). Our interpretation is analogous: There is one effect that affects oxygen and the quenching process and a second one that affects the luminophore itself.

Increased hydrostatic pressure causes the sensing membrane's c_{O_2} to decrease as a result of a shift in the membrane–seawater equilibrium [Eq. (16)]. At the same time, the sensing membrane is compressed, which increases its viscosity and thus affects the quenching efficiency. The sum of these processes results in higher lifetimes (phase shift, phase delay) and apparently less seawater O_2.

Simultaneously, the luminophore properties are affected by hydrostatic pressure. Compression of the sensing membrane (i.e., the matrix) increases the energy level of the luminophore. It seems that, in relative terms, the luminophore's excited state is more strongly affected than the ground state so that the tendency to return to the ground state is increased. The (excited state's) lifetime is therefore slightly reduced at high pressures.

Both the O_2-dependent effect (changed sensing membrane equilibrium concentration and altered quenching efficiency) and the O_2-independent effect (altered luminophore properties) act in parallel but opposite directions and are always superimposed.

Previous parameterizations of the pressure response focused on the O_2-dependent part [see Eqs. (1) and (2)]. To derive equations for both the O_2-dependent
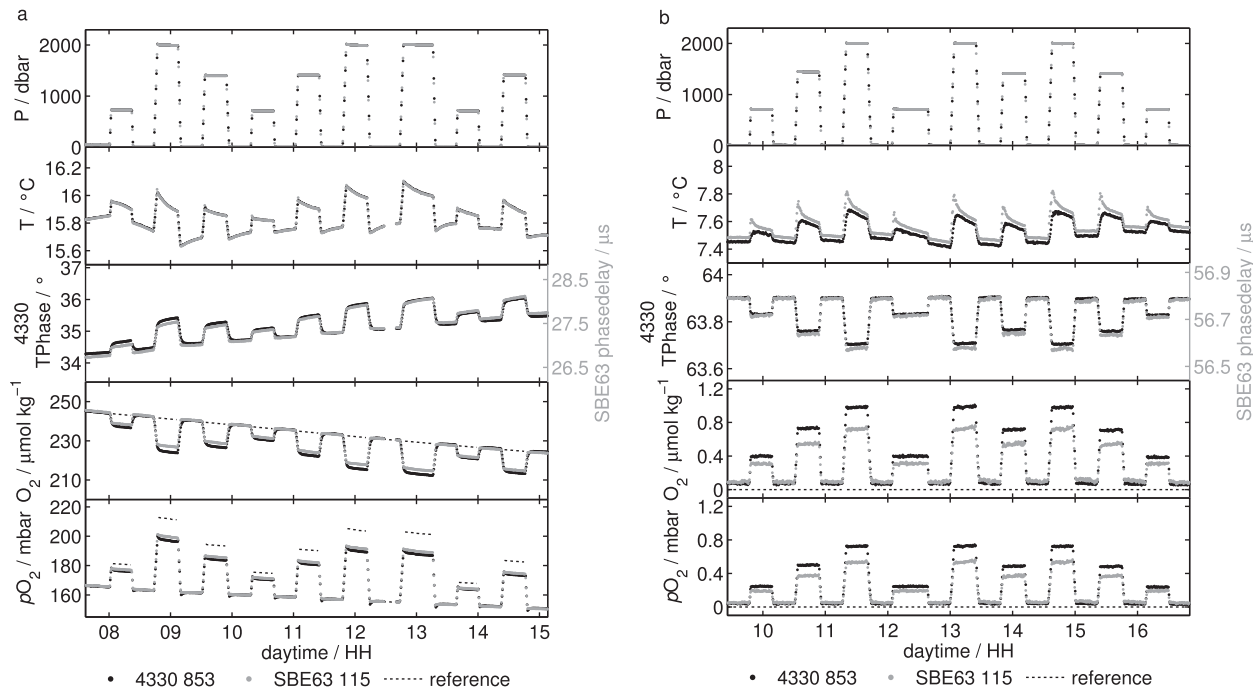
FIG. 3. Response to hydrostatic pressure of an Aanderaa optode (4330 853, black dots) and a Sea-Bird optode (SBE63 115, gray dots) at (a) high O_2 (ca. 16°C and 80% O_2 saturation) and (b) zero O_2 (ca. 8°C). (from top to bottom) Pressure, temperature, lifetime, O_2 concentration, and O_2 partial pressure. Pressure levels are at 700, 1400, and 2000 dbar, respectively. In (a) at high O_2, the luminophore's lifetime (phase shift, phase delay) is *increased* under pressure. Consequently, the temperature—but not pressure—compensated optode O_2 (concentration $c_{O_2,raw}$ or partial pressure $pO_{2,raw}$) underestimates the actual O_2 level (dashed; see text for discussion of the decreasing O_2 trend). In (b) in the absence of O_2, the luminophore's lifetime is *decreased*. Consequently, the temperature—but not pressure—compensated optode O_2 ($c_{O_2,raw}$, $pO_{2,raw}$) overestimates the actual (zero) O_2 level (dashed).

and O_2-independent parts, we need to reconsider the order in which the functional model parts are applied. The "classical" approach is described as follows.

step 1a: Compensate for the temperature dependence of quenching, that is, convert the raw sensor phase shift φ_{raw} to a (raw) oxygen quantity ($c_{O_2,raw}$ or $pO_{2,raw}$).

step 1b: Compensate for the pressure dependence of quenching, that is, convert the raw oxygen quantity to a fully corrected one.

The alternative approach would be to deal with the pressure dependence first (raw phase shift to corrected phase shift) and then correct the temperature dependence (corrected phase shift to fully corrected O_2). While this order is in principle feasible, it is less straightforward to arrive at simple parameterizations.

Based on the work presented here, we propose to expand the classical scheme by an additional step to first deal with the pressure effect on the luminophore and then with the quenching process itself.

step 0: Compensate for the O_2-independent pressure effect on the luminophore, that is, convert the raw phase shift φ_{raw} to a pressure-adjusted one φ_{adj}.

step 1a: Compensate for the temperature dependence of quenching, that is, convert the adjusted phase shift φ_{adj} to an adjusted oxygen quantity.

step 1b: Compensate for the pressure dependence of quenching, that is, convert the adjusted oxygen quantity to a fully corrected one.

c. Quantification

At zero O_2, only the O_2-independent pressure effect is visible as an offset to unpressurized (surface) conditions. The phase offset and O_2 concentration offset are linear with pressure, while the pO_2 offset follows an exponential trend (Fig. 4a). In contrast to the c_{O_2} and pO_2 offset, the phase offset is nearly temperature independent. Moreover, the phase offset is homogeneous within the Aanderaa and Sea-Bird optodes (Fig. 4b). To compensate for the O_2-independent pressure response of the luminophore, the phase shift φ needs to be adjusted according to

$$\varphi_{adj} = \varphi_{raw} + z\,P, \qquad (17)$$

where z is a phase offset of 0.1° per 1000 dbar for the Aanderaa optodes and 0.115 μs per 1000 dbar for the
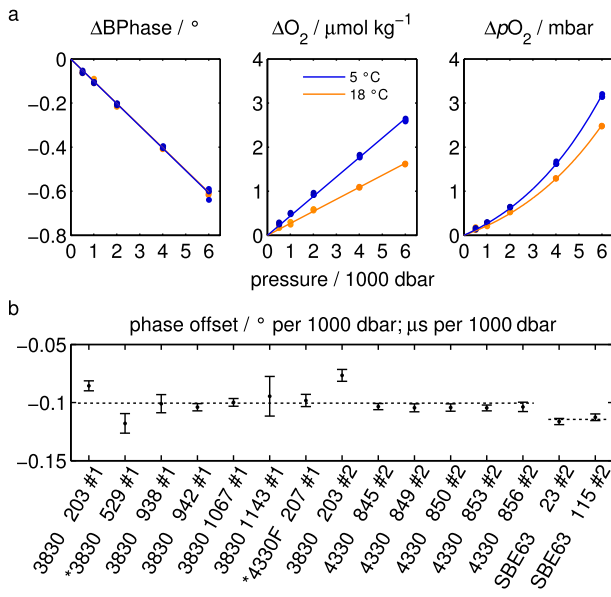
FIG. 4. Oxygen-independent optode pressure response. (a) Change in (left) phase shift, (middle) O_2 concentration, and (right) pO_2 of optode 3830 938. Only the change in phase shift is temperature independent. (b) Phase offset (change in phase shift vs pressure) for all optodes. The asterisk denotes the two optodes used in the field experiment.

SBE63 optodes. Despite using the same PSt3 sensing foil (PreSens GmbH), phase shifts are different between the manufacturers since a different excitation frequency of the luminophore is used (5000 vs 3840 Hz, respectively).

The O_2-dependent part (Fig. 5) shows a downward-curved relation in phase offset (phase ratios are inhomogeneous between sensors) and a closely linear trend in the c_{O_2} ratio, as well as the pO_2 ratio with the same slope f. The qualitative picture is the same for the classical approach of neglecting the O_2-independent part (Fig. 5a) and the revised approach with a preceding phase offset adjustment according to Eq. (17) (Fig. 5c). In both cases, the slope f increases with temperature.

The magnitude of the O_2 reduction matches the magnitude of the equilibrium effect. However, the temperature dependence follows opposite trends, indicating the presence of additional processes. Because of a lack of characterization of these additional processes, we chose to follow a simplistic linear parameterization according to Eq. (1) rather than to empirically adjust Eq. (16) [or Eq. (2)] for the observed temperature dependence.

Except for optode 4330 856, the slope f is in the same range for all Aanderaa optodes (Figs. 5b,d), despite the broad range of sensor (foil) age and deployment history. Without phase adjustment—that is, following the classical approach—there is, however, a difference between Aanderaa and SBE63 optodes (ratio of f ca. 0.9).

With the preceding phase offset adjustment, this difference vanishes (ratio of f of 1.0, see Fig. 6). In fact, an analogous pressure response of the quenching process can be expected since both the SBE63 optodes and the Aanderaa optodes with standard foil use the same coated PSt3 sensing membrane material and luminophore. This supports the physical credibility of the proposed new approach to split the pressure response into two separate steps.

The temperature dependence of the O_2-dependent pressure effect is shown in Fig. 6 with f being higher at higher temperatures. The temperature slope is very similar between sensors, while there is some variation in the offset ($\pm 0.2\%$ per 1000 dbar). With the classical approach, f has an average of 3.3% per 1000 dbar at 1°C that is very close to the 3.2% per 1000 dbar of Uchida et al. (2008). The factor f for the SBE63 is lower by ca. 0.3% per 1000 dbar. With a preceding phase offset, f is about 4.2% per 1000 dbar at 1°C and the Aanderaa and Sea-Bird optodes follow the same trend. Parameters from the laboratory experiment are summarized in Table 2.

There are, however, two caveats to these results: Only two SBE63 optodes were available and their pressure range was limited to 2000 dbar, which somewhat limits the significance of the comparison. The parameters for the SBE63 optodes might thus need to be refined based on further experiments. Moreover, the only fast-response foil (optode 4330F 207) showed a slightly higher O_2-dependent pressure response using the revised scheme than the average of the standard foil Aanderaa optodes. Still, it is well within the range of variability of the standard foil optodes and thus not treated separately.

d. Laboratory validation

A third laboratory experiment was performed with three Aanderaa optodes at ca. 80% O_2 up to a pressure of 2000 dbar. As no data were obtained at zero O_2, this experiment was not included to derive the pressure response. It can thus be used to validate the mean parameterization (Table 2) under laboratory conditions.

Using a constant f of 3.2% per 1000 dbar (Uchida et al. 2008), the mean absolute bias is 0.56% per 1000 dbar. This is reduced to 0.15% per 1000 dbar by inclusion of the temperature dependence of f (Table 2, upper parameter set). With the revised scheme (Table 2, lower parameter set), the error comes down to 0.18% per 1000 dbar.

e. Field experiment

Under field conditions, a clear distinction between O_2-independent pressure effect, O_2-dependent pressure effect, and its temperature dependence is not possible. Therefore, we will use the phase offset z and the temperature slope of f from the laboratory experiments
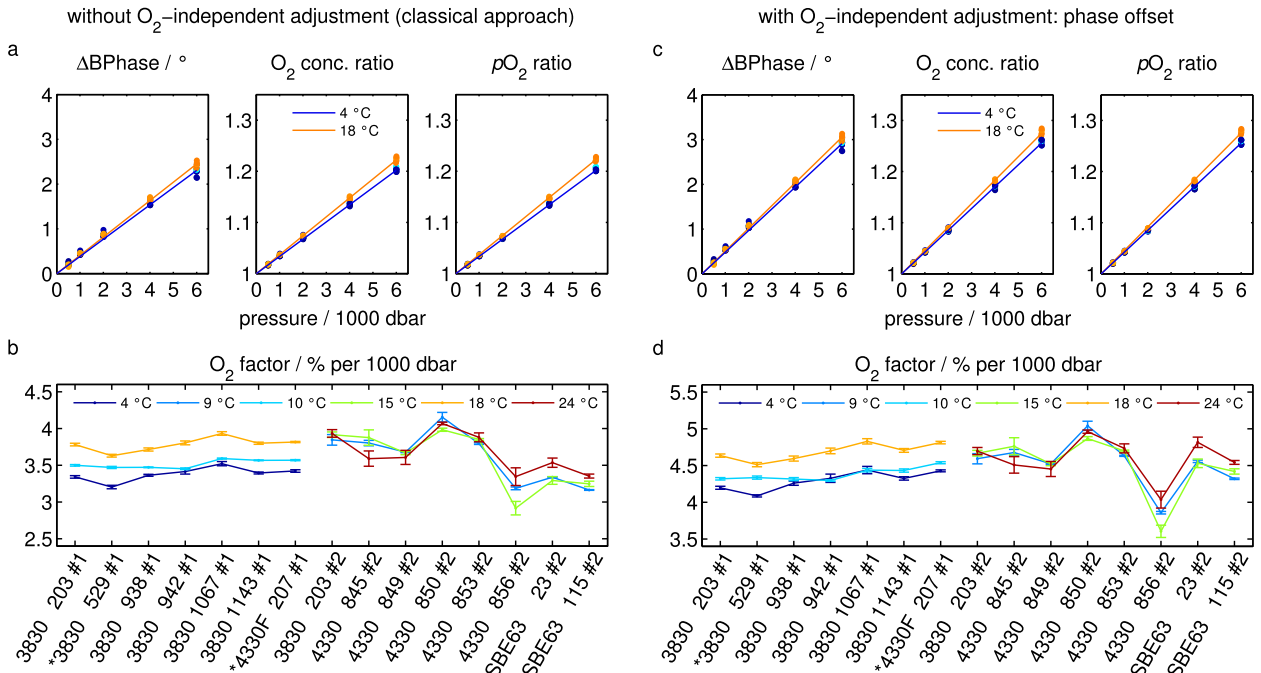
FIG. 5. Oxygen-dependent optode pressure response (a),(b) without preceding O_2-independent adjustment and (c),(d) with a phase offset adjustment. (a),(c) Change in (left) phase shift offset, (middle) O_2 concentration ratio $c_{O_2}/c_{O_2,\text{raw}}$, and (right) partial pressure ratio $pO_2/pO_2,\text{raw}$ of optode 3830 938. (b),(d) Oxygen pressure factor (slope of O_2 ratio vs pressure) for all optodes and both experiments. The phase offset adjustment increases the apparent O_2-dependent pressure effect by 1%. In parallel, the difference in the O_2 factor f between Aanderaa and SBE63 optodes vanishes when preceded by the O_2-independent phase offset adjustment. The asterisk denotes the two optodes used in the field experiments.

(Table 2), which were uniform between sensors, and only allow the zero intercept of f to be adjusted according to the field data.

A qualitative picture of the uncompensated pressure effect is given in Fig. 2. The apparent linear slope for the 3830 529 and 4330F 207 optodes is eliminated with an f intercept of 3.2% and 3.6% per 1000 dbar using the classical approach (Fig. 7, left panels) and of 4.0% and 4.5% per 1000 dbar using the revised approach (Fig. 7, right panels), respectively. This mirrors the laboratory observations with the optode 3830 529 being at the low end and the optode 4330F 207 being at the high end of the O_2-dependent pressure effect (Figs. 5b,d) and thus confirms the laboratory results.

Quantitatively, the median absolute residuals for the 3830 and 4330F optodes are quite similar between the calculation schemes: 0.66 and 1.06 μmol kg^{-1} for the classical approach and 0.65 and 1.03 μmol kg^{-1} for the revised approach, respectively. Here, the classical approach benefits from the very narrow temperature range (Fig. 2) so that the unaccounted temperature dependence does not appear strongly in the residuals. The revised approach performs at least as good as the classical correction in this example. However, it includes improved knowledge about the pressure behavior

of optodes and is expected to yield better results in other ocean settings.

f. Pressure correction uncertainty

The uncertainty of the pressure correction consists of two parts. One part is the adequacy of the parameterization and the other part is the uncertainty of the respective coefficients. Based on the laboratory and field evidence, an empirical, linear parameterization seems appropriate. The proposed new scheme incorporates mechanistic elements although the O_2-dependent part remains empirical as the interplay between equilibrium effect and changes in quenching efficiency is not yet fully understood.

As for the coefficients, the largest part of the pressure correction uncertainty stems from the variability between sensors themselves (ca. 0.2% per 1000 dbar). Based on the laboratory validation, the practical uncertainty amounts to 0.2% per 1000 dbar for both the classical approach and the newly proposed approach (Table 2, upper and lower parameter sets, respectively). The field experiment, too, indicates an uncertainty of 0.2% per 1000 dbar. Given that the same sensors were used in the laboratory experiment 1 and field experiment, we deem a slightly more conservative overall uncertainty of 0.3% per 1000 dbar realistic.
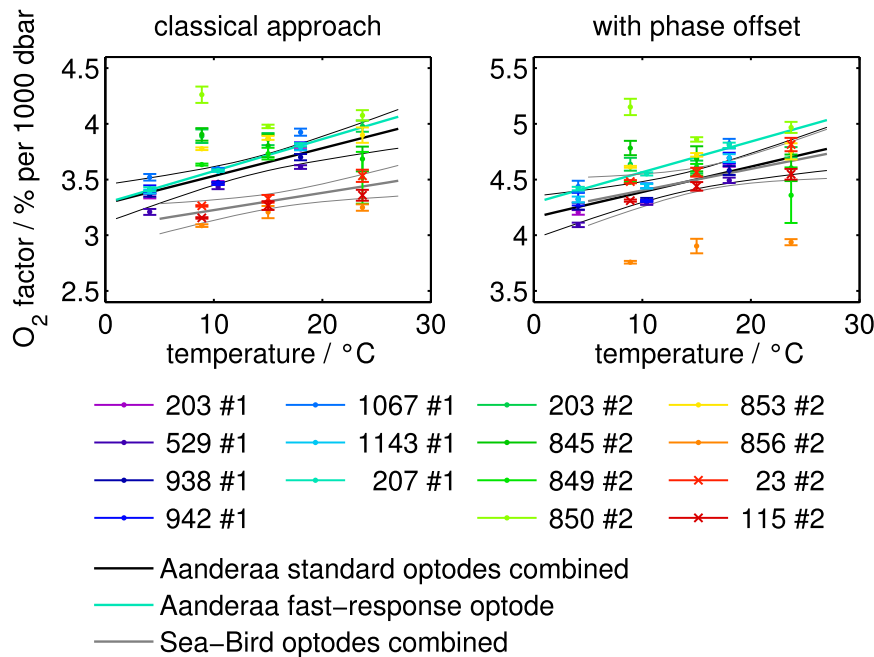
FIG. 6. Temperature dependence of the O_2 factor f using the (left) classical approach with a O_2 factor only and (right) with preceding O_2-independent phase offset adjustment. Optodes are color coded and grouped in Aanderaa optodes (dots) and Sea-Bird SBE63 optodes (crosses). The phase offset adjustment reduces the mismatch between experiments 1 and 2 at lower temperatures. Lines denote linear fits for all Aanderaa optodes with standard foil (black), the Aanderaa optode with fast-response foil (cyan), and both Sea-Bird optodes (gray) (with confidence bounds for combined fits).

This level of uncertainty needs to be taken into account when considering an optode drift correction/calibration based on the comparison to a climatological reference at depth (e.g., Takeshita et al. 2013). For a typical Argo O_2 float with 2000 dbar profiling depth, this amounts to half a percent uncertainty on top of the uncertainty of the climatology itself. This may exceed the desired level of accuracy, for example, for air–sea gas exchange and eventually net community production calculations. A better constraint for this kind of work is derived from direct in-air measurements (Bittig and Körtzinger 2015).

5. Summary

Oxygen optodes show a systematic pressure response: With increased hydrostatic pressure, they generally read lower O_2 than in the ambient seawater. Foremost, this is due to the effect of pressure on the equilibrium between the optode sensing membrane and seawater. Because of a higher partial molar volume of O_2 in the membrane, equilibrium concentrations are actually reduced under pressure, which causes the optodes to read a lower O_2. In contrast, hydrostatic pressure influences the quenching process only to a minor degree

(see section 2b; Taylor 1978; Ludwig and Macdonald 2005). However, the luminophore itself shows a pressure effect that acts in the opposite direction of the equilibrium effect. Consequently, optodes read slightly too high at O_2 levels below ca. 5% O_2 saturation, while the equilibrium effect dominates above this level and optodes read too low.

The pressure response shows an O_2 dependence that is closely linear with O_2, both for Aanderaa and Sea-Bird optodes. Its magnitude is somewhat temperature dependent and there is no pressure hysteresis.

Because of the combination of a pressure impact on the luminophore besides the impact on O_2 equilibrium

TABLE 2. Pressure response parameterizations based on the laboratory experiments. The upper set gives parameters for the classical approach [Eq. (1) only] and the lower set for the revised approach with phase adjustment [Eqs. (17)–(19)]. The uncertainty of f is about 0.3% per 1000 dbar.

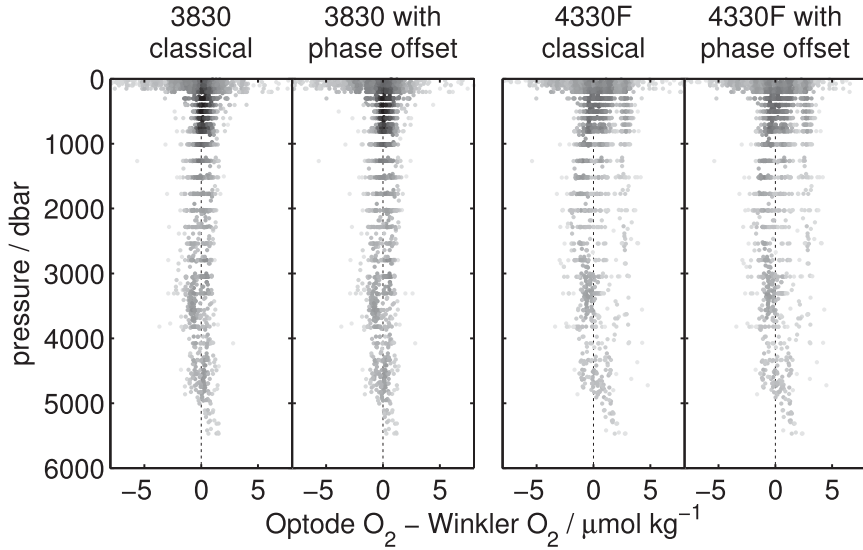|	z per 1000 dbar	f / % per 1000 dbar
Aanderaa	0°	$3.28 + 0.025\vartheta$
SBE63	0 μs	$3.07 + 0.016\vartheta$
Aanderaa	0.100°	$4.19 + 0.022\vartheta$
SBE63	0.115 μs	$4.19 + 0.022\vartheta$

FIG. 7. Residuals after pressure correction for Aanderaa optode models 3830 and 4330F of R/V *Polarstern* cruise ANT-XXVII/2. (left) Correction following the classical approach [(Eq. (1)]. (right) Correction following the revised approach [Eqs. (17)–(19)]. The shading indicates the data density.

concentrations and quenching, we propose a new optode calculations scheme. In this scheme, we first deal with changes to the luminophore caused by pressure (step 0) before addressing oxygen quenching (step 1).

step 0. Compensate for the O_2-independent pressure effect on the luminophore.

The measured raw phase shift φ_{raw} is pressure corrected to an adjusted one φ_{adj} according to

$$\varphi_{adj} = \varphi_{raw} + z\,P,$$

where the phase offset z depends on the manufacturer (Table 2, lower parameter set).

step 1a. Compensate for the temperature dependence of quenching.

Application of a functional model $\mathscr{F}$ for the temperature dependence of quenching converts the adjusted phase shift φ_{adj} to an adjusted oxygen quantity, that is,

$$
\begin{aligned}
c_{O_2,adj} &= \mathscr{F}_c(\vartheta, \varphi_{adj}) \quad \text{or} \\
pO_{2,adj} &= \mathscr{F}_p(\vartheta, \varphi_{adj}).
\end{aligned}
\tag{18}
$$

It depends on the functional model $\mathscr{F}$ whether the oxygen quantity is a concentration $c_{O_2,adj}$ or a partial pressure $pO_{2,adj}$.

step 1b. Compensate for the pressure dependence of quenching.

The adjusted oxygen quantity is converted to a fully corrected one by accounting for the pressure effect on quenching, that is,

$$c_{O_2} = c_{O_2,adj}[1 + f(\vartheta)\,P] \quad \text{or}$$

$$pO_2 = pO_{2,adj}[1 + f(\vartheta)\,P]\exp\left[\frac{V_m^L(O_2)\,P}{R(\vartheta + 273.15\,\text{K})}\right],$$
$$\tag{19}$$

where $f(\vartheta)$ is a temperature-dependent factor that is uniform for both Aanderaa and Sea-Bird optodes (see Table 2, lower parameter set). Here, the pO_2 increase because of hydrostatic pressure (see section 2a) is dealt with explicitly and outside of $\mathscr{F}$. It depends on the functional model of the temperature dependence whether this is already included in $\mathscr{F}$. The proposed scheme is physically plausible: Both Aanderaa and Sea-Bird use sensing membranes from the same manufacturer but apply different excitation frequencies. This is mirrored in an analogous O_2 quenching effect but different phase shift offset of the luminophore. Whenever possible, this scheme should be applied to O_2 optode data to properly account for the two opposing pressure effects. If for some (practical) reason, however, the raw phase φ_{raw} is not available, then a reasonable pressure correction is still feasible since the O_2 effect dominates in most applications. If both processes are lumped together, then the pressure correction is reduced to Eq. (19) and the upper parameter set of Table 1 is used for

$f(\vartheta)$ (note the difference between Aanderaa and Sea-Bird optodes).

There is some variation (offset in f) in the pressure response between sensors on the order of 0.2% per 1000 dbar. This is the most important contributor to the uncertainty of our pressure correction, which is estimated at 0.3% per 1000 dbar.

Moreover, the pressure effect might drift with time as has been seen for the temperature dependence of optodes (Bittig and Körtzinger 2015). Given the broad age range of optodes, especially during experiment 1, the small range of f is encouraging and suggests that aging is of minor importance. Still, a tendency toward lower f with age could be deduced from experiment 1 (Figs. 5b,d). However, we believe this is exceeded by intrinsic variability between sensors (see experiment 2).

APPENDIX

Pressure Dependence of the Partial Pressure

The discussion of the chemical potential μ in section 2b can be expanded to derive the pressure dependence of the partial pressure pO_2 [Eq. (7)]. Enns et al. (1965) describe an experiment in which a gas phase $(^G)$ at ambient (air) pressure is in equilibrium with a pressurized liquid $(^L)$. For a gas dissolved in a liquid, the chemical potential follows Henry's law, that is,

$$\mu_i^L = \mu_i^{*,L} + RT \ln a_i.$$

For the gas phase, the chemical potential follows Raoult's law, that is,

$$\mu_i^G = \mu_i^{\circ,G} + RT \ln p_i, \qquad (A1)$$

where $\mu_i^{\circ,G}$ is the chemical potential of the standard state at the same temperature and pressure according to Raoult's law, that is, the pure gas.

In equilibrium,

$$\mu_i = \mu_i^{*,L} + RT \ln a_i = \mu_i^{\circ,G} + RT \ln p_i. \qquad (A2)$$

Upon pressurization of the liquid, μ_i changes according to Eq. (10). With Eq. (A2), this gives

$$\left(\frac{\partial \mu_i}{\partial P}\right)_T = V_{m,i}^L = \left(\frac{\partial \mu_i^{\circ,G}}{\partial P}\right)_T + RT \left(\frac{\partial \ln p_i}{\partial P}\right)_T. \qquad (A3)$$

The standard state of the gas phase μ_i° is unaffected by the pressurization of the liquid, that is, $\partial \mu_i^{\circ,G}/\partial P = 0$, and the pressure-dependent change in μ_i needs to be compensated for by a change in the partial pressure p_i. Integration from $P = 0$ dbar yields the dependence of partial pressure p_i on hydrostatic pressure P [Eq. (7)].

REFERENCES

Aanderaa Data Instruments, 2009: Operating manual: Oxygen optode 4330, 4835. Tech. Doc. 269, 71 pp.

Bittig, H. C., and A. Körtzinger, 2015: Tackling oxygen optode drift: Near-surface and in-air oxygen optode measurements on a float provide an accurate in situ reference. *J. Atmos. Oceanic Technol.*, **32**, 1536–1543, doi:10.1175/JTECH-D-14-00162.1.

——, B. Fiedler, T. Steinhoff, and A. Körtzinger, 2012: A novel electrochemical calibration setup for oxygen sensors and its use for the stability assessment of Aanderaa optodes. *Limnol. Oceanogr. Methods*, **10**, 921–933, doi:10.4319/lom.2012.10.921.

——, ——, R. Scholz, G. Krahmann, and A. Körtzinger, 2014: Time response of oxygen optodes on profiling platforms and its dependence on flow speed and temperature. *Limnol. Oceanogr. Methods*, **12**, 617–636, doi:10.4319/lom.2014.12.617.

Carey, F. G., and Q. H. Gibson, 1976: The activity of dissolved oxygen at 1000 atm hydrostatic pressure. *Deep-Sea Res. Oceanogr. Abstr.*, **23**, 1215–1216, doi:10.1016/0011-7471(76)90898-6.

Enns, T., P. F. Scholander, and E. D. Bradstreet, 1965: Effect of hydrostatic pressure on gases dissolved in water. *J. Phys. Chem.*, **69**, 389–391, doi:10.1021/j100886a005.

Fennel, K., I. Cetinic, E. D'Asaro, C. Lee, and M. J. Perry, 2011: Autonomous data describe North Atlantic spring bloom. *Eos, Trans. Amer. Geophys. Union*, **92**, 465–466, doi:10.1029/2011EO500002.

Garcia, H. E., and L. I. Gordon, 1992: Oxygen solubility in seawater: Better fitting equations. *Limnol. Oceanogr.*, **37**, 1307–1312, doi:10.4319/lo.1992.37.6.1307.

Glueckauf, E., 1951: The composition of atmospheric air. *Compendium of Meteorology*, T. F. Malone, Ed., Amer. Meteor. Soc., 3–12.

Johnson, K. S., and Coauthors, 2009: Observing biogeochemical cycles at global scales with profiling floats and gliders: Prospects for a global array. *Oceanography*, **22**, 216–225, doi:10.5670/oceanog.2009.81.

——, S. C. Riser, and D. M. Karl, 2010: Nitrate supply from deep to near-surface waters of the North Pacific subtropical gyre. *Nature*, **465**, 1062–1065, doi:10.1038/nature09170.

Jordan, S. M., and W. J. Koros, 1990: Permeability of pure and mixed gases in silicone rubber at elevated pressures. *J. Polym. Sci.*, **28B**, 795–809, doi:10.1002/polb.1990.090280602.

Kamiya, Y., Y. Naito, T. Hirose, and K. Mizoguchi, 1990: Sorption and partial molar volume of gases in poly (dimethyl siloxane). *J. Polym. Sci.*, **28B**, 1297–1308, doi:10.1002/polb.1990.090280808.

——, ——, K. Terada, K. Mizoguchi, and A. Tsuboi, 2000: Volumetric properties and interaction parameters of dissolved gases in poly(dimethylsiloxane) and polyethylene. *Macromolecules*, **33**, 3111–3119, doi:10.1021/ma991536b.

Lakowicz, J. R., Ed., 2006: *Principles of Fluorescence Spectroscopy.* 3rd ed. Springer, 954 pp., doi:10.1007/978-0-387-46312-4.

Ludwig, H., and A. G. Macdonald, 2005: The significance of the activity of dissolved oxygen, and other gases, enhanced by high hydrostatic pressure. *Comp. Biochem. Physiol.*, **140A**, 387–395, doi:10.1016/j.cbpb.2005.02.001.

McNeil, C. L., and E. A. D'Asaro, 2014: A calibration equation for oxygen optodes based on physical properties of the sensing foil. *Limnol. Oceanogr. Methods*, **12**, 139–154, doi:10.4319/lom.2014.12.139.

Rohardt, G., E. Fahrbach, and A. Wisotzki, 2011: Physical oceanography during POLARSTERN cruise ANT-XXVII/2. Helmholtz Center for Polar and Marine Research, Alfred Wegener Institute, doi:10.1594/PANGAEA.772244.

Sea-Bird Electronics, 2013: SBE63 optical dissolved oxygen sensor user's manual. 46 pp.

Takeshita, Y., T. R. Martz, K. S. Johnson, J. N. Plant, D. Gilbert, S. C. Riser, C. Neill, and B. Tilbrook, 2013: A climatology-based quality control procedure for profiling float oxygen data. *J. Geophys. Res. Oceans*, **118**, 5640–5650, doi:10.1002/jgrc.20399.

Taylor, C. D., 1978: The effect of pressure upon the solubility of oxygen in water: Implications of the deviation from the ideal gas law upon measurements of fluorescence quenching. *Arch. Biochem. Biophys.*, **191**, 375–384, doi:10.1016/0003-9861(78)90101-7.

Tengberg, A., and Coauthors, 2006: Evaluation of a lifetime-based optode to measure oxygen in aquatic systems. *Limnol. Oceanogr. Methods*, **4**, 7–17, doi:10.4319/lom.2006.4.7.

Thierry, V., D. Gilbert, T. Kobayashi, and C. Schmid, 2013: Processing Argo oxygen data at the DAC level, version 1.3. Argo Data Management, 20 pp. [Available online at http://www.argodatamgt.org/content/download/16300/106561/file/ARGO_oxygen_proposition_v1p3.pdf.]

Uchida, H., T. Kawano, I. Kaneko, and M. Fukasawa, 2008: In situ calibration of optode-based oxygen sensors. *J. Atmos. Oceanic Technol.*, **25**, 2271–2281, doi:10.1175/2008JTECHO549.1.

——, G. C. Johnson, and K. E. McTaggart, 2010: CTD oxygen sensor calibration procedures. GO-SHIP repeat hydrography manual: A collection of expert reports and guidelines, E. M. Hood, C. L. Sabine, and B. M. Sloyan, Eds., IOCCP Rep. 14, ICPO Publication Series 134, 17 pp. [Available online at http://www.go-ship.org/HydroMan.html.]

Weiss, R. F., and B. A. Price, 1980: Nitrous oxide solubility in water and seawater. *Mar. Chem.*, **8**, 347–359, doi:10.1016/0304-4203(80)90024-9.